# A combined temperature-dependent electron and single-crystal X-ray diffraction study of the fresnoite compound $Rb_2V^{4+}V_2^{5+}O_8$

Ray L. Withers,[a,*] Thomas Höche,[b] Yun Liu,[a] Saeid Esmaeilzadeh,[c]
Ralf Keding,[d] and Brian Sales[e]

[a] *Research School of Chemistry, The Australian National University, Building 35, Science Rd., ACT, 0200, Canberra, Australia*
[b] *Leibniz-Institut für Oberflächenmodifizierung e.V., Permoserstrasse 15, D-04318 Leipzig, Germany*
[c] *Department of Inorganic Chemistry, Arrhenius Laboratory, Stockholm University, S-106 91 Stockholm, Sweden*
[d] *Otto-Schott-Institut für Glaschemie, Friedrich-Schiller-Universität, Fraunhoferstrasse 6, D-07743 Jena, Germany*
[e] *Oak Ridge National Laboratory, Oak Ridge, TN 37831, USA*

## Abstract

High-purity $Rb_2V_3O_8$ has been grown and temperature-dependent electron and single-crystal X-ray diffraction used to carefully investigate its fresnoite-type reciprocal lattice. In contrast to other recently investigated representatives of the fresnoite family of compounds, $Rb_2V_3O_8$ is not incommensurately modulated with an incommensurate basal plane primary modulation wave vector given by $\mathbf{q} \sim 0.3 \langle 110 \rangle^*$. A careful low-temperature electron diffraction study has, however, revealed the existence of weak incommensurate satellite reflections characterized by the primitive primary modulation wave vector $\mathbf{q}_1 \sim 0.16\mathbf{c}^*$. The reciprocal space positioning of these incommensurate satellite reflections, the overall $(3+1)$-$d$ superspace group symmetry, as well as the shapes of the refined displacement ellipsoids determined from single-crystal XRD refinement, are all consistent with their arising from a distinct type of condensed rigid unit modes (RUMs) of distortion of the $Rb_2V_3O_8$ parent structure.
$\copyright$ 2004 Elsevier Inc. All rights reserved.

*Keywords:* $Rb_2V_3O_8$ fresnoite; Low-temperature incommensurate phase transition; Frozen RUM mode; Temperature-dependent electron diffraction study; Low-temperature average structure refinement

## 1. Introduction

The average, or parent, *P4bm* framework crystal structure of the mineral fresnoite, $Ba_2TiSi_2O_8$ (BTS), is comprised of essentially rigid, corner-connected $SiO_4$ tetrahedra and $TiO_5$ square pyramids arranged in (001) sheets interspersed by layers of Ba ions [1–3] (see Fig. 1). Compounds belonging to this fresnoite structure type include $Ba_2TiGe_2O_8$ (BTG) [4–6], $Sr_2TiSi_2O_8$ (STS) [7,8], $Ba_2VSi_2O_8$ (BVS) [9–11], $K_2V_3O_8$ [12,13], $Rb_2V_3O_8$ [13], $Cs_2V_3O_8$ [14] and $(NH_3)_2V_3O_8$ [13]. BTS, BTG, STS and BVS are of interest as a result of their piezoelectric and pyroelectric properties [4,5,15–17], while the $A_2V_3O_8$ family of compounds

has attracted recent attention due to their novel low-temperature magnetic properties (associated with the presence of magnetic $V^{4+}$ ions in the square pyramidal sites), as well as their nonlinear optical properties [13,18,19].

From the structural and crystal chemical point of view, fresnoites are challenging as a result of their inherent susceptibility to displacive structural phase transitions [5,15–18,20–22]. Each of the fresnoites BTS, BTG, STS and BVS, for example, are now known to undergo a high-temperature phase transition into either a $(3+1)$-$d$ (in the case of BTG) or a $(3+2)$-$d$ (in the cases of BTS, STS and BVS) incommensurately modulated room temperature structure [6–8,11,22]. These incommensurately modulated structures are characterized by having essentially the same in-plane primary modulation wave-vector component ($\mathbf{q} \sim 0.30$

*Corresponding author. Fax: +61-2-6125-0750.
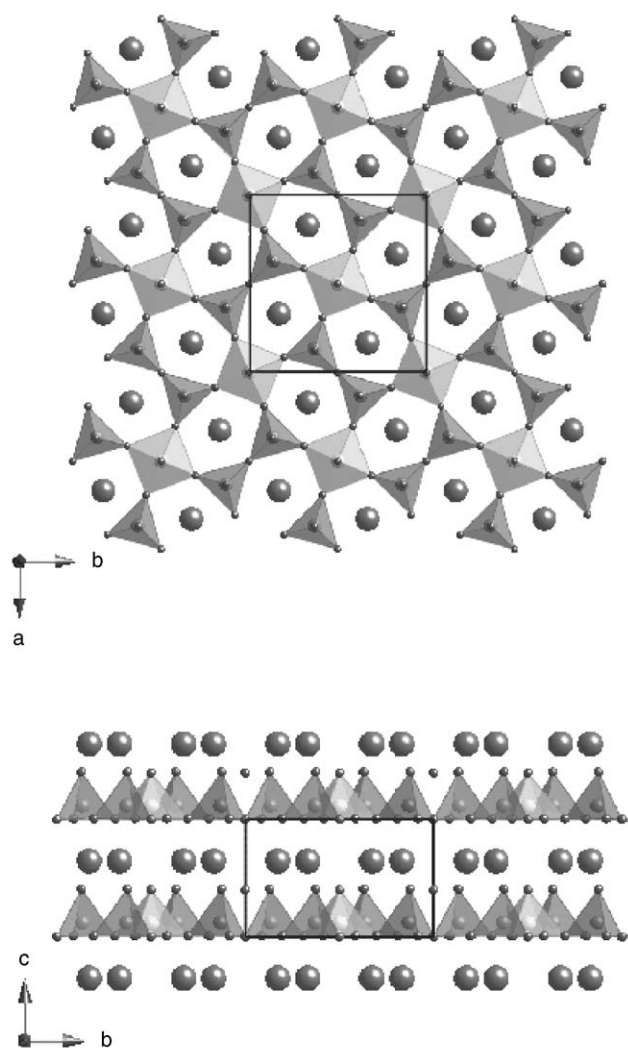*E-mail address:* withers@rsc.anu.edu.au (R.L. Withers).

Fig. 1. The *P4bm* ideal fresnoite structure with its characteristic layers of essentially rigid, corner-connected $TO_4$ ($T$ = Si, Ge or V) tetrahedra (darker shading) and $MO_5$ ($M$ = Ti or V) square pyramids (lighter shading) interspersed with layers of Ba, Sr or Rb ions (the large balls) is shown in projection down the [001] direction in (a) and the [100] direction in (b).



Fig. 2. A scanning electron micrograph of the as-grown plate-like $Rb_2V_3O_8$ single crystals.

$\langle 110 \rangle_p^*$) and displacement eigenvectors involving rotation of the constituent tetrahedra and square pyramids around $c$ in combination with appropriate in-plane translations [6,22].

A plausible crystal chemical explanation for this observed behavior was suggested by a recent rigid unit mode (RUM) analysis of the inherent displacive structural flexibility of the ideal fresnoite framework structure type [22], which found a zero-frequency RUM mode involving rotation of the constituent tetrahedra and square pyramids around $c$ in combination with appropriate in-plane translations existing, but only for the very specific in-plane modulation wave vector/s $\mathbf{q} \sim 0.30 \langle 110 \rangle_p^*$. The presence of this particular RUM mode in each of BTG, BTS, STS and BVS suggests that
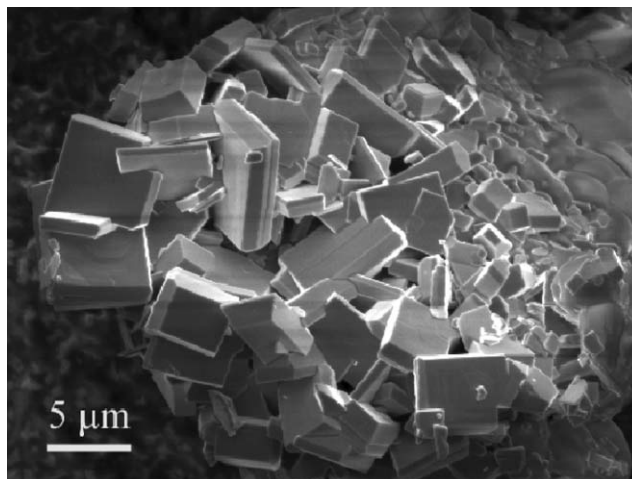
it might well be a universal phenomenon and present in all fresnoite-type compounds. It is therefore important from the crystal chemical point of view to investigate whether or not this is indeed the case. The purpose of the current paper is to present the results of a search for the presence or otherwise of such condensed RUM modes in the fresnoite $Rb_2V_3O_8$.

## 2. Experimental

High-purity $Rb_2V_3O_8$ was prepared by the controlled reduction of $V_2O_5$ with RbI, following the route proposed by Ha-Eierdanz and Müller [23], i.e.

$$2RbI + 2V_2O_5 \rightarrow Rb_2V_3O_8 + \text{``}VO_2\text{''} + I_2.$$
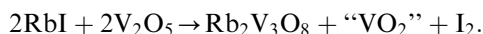
A 1:1 (molar ratio) mixture of $V_2O_5$ and RbI was sealed in an evacuated quartz glass ampoule and annealed at 500°C for 2 weeks. The ampoule was placed in the tube furnace in such a way that the mixed powder (at one end of the ampoule) was positioned in the hot zone of the furnace, while the other end was left sticking out of the furnace. In the latter colder part of the ampoule, iodine was found to condense, while at the other hot end tiny $Rb_2V_3O_8$ single crystals of about 5 μm edge length grew (see Fig. 2). The surplus vanadium, "$VO_2$" in the above equation, was not directly detected but was presumed, following Ha-Eierdanz and Müller [23], to be transported via sublimation or chemical transport reaction to the colder end of the tube.

Transmission electron microscope (TEM) analysis was carried out in a Philips EM 430 TEM on crushed grains of the tiny $Rb_2V_3O_8$ crystals dispersed onto holey carbon-coated copper grids. The low-temperature studies were carried out on a Gatan liquid nitrogen cold stage at liquid nitrogen temperature. Only quite limited

tilt ($\sim \pm 10°$) was available about one axis and the microscope and stage used were unsuitable for high resolution electron microscopy (HREM) imaging.

Differential scanning calorimetry (DSC) was performed using a Thermal Analyst 2100 (TA Instruments Inc.) in the temperature range from liquid nitrogen up to 40°C. The rate of temperature increase was 5°C/min. Powders were heat treated at 120°C for 5 h prior to DSC measurement to remove adsorbed water.

Although the $Rb_2V_3O_8$ crystals prepared by the controlled reduction of $V_2O_5$ with RbI were suitable for electron diffraction investigation, larger single crystals were required for single-crystal X-ray diffraction study. $Rb_2V_3O_8$ single crystals were thus also grown by cooling appropriate amounts of $VO_2$ in a molten $RbVO_3$ flux in a platinum crucible sealed inside a silica container [18,24]. The resulting high-quality plate-like crystals attained an edge length of up to 2 mm at a thickness of some tenths of millimetres and were used for the low-temperature single-crystal X-ray study after crushing.

## 3. Results and discussion

### 3.1. Electron diffraction

Given that incommensurate satellite reflections have previously been observed at the $\mathbf{G} \pm \sim 0.30 \langle 110 \rangle_p^* + \frac{1}{2}\mathbf{c}_p^*$ (G a parent $P4bm$ Bragg reflection, subscript p for parent) positions of reciprocal space in the cases of BTG, BTS and BVS, and at both the $\mathbf{G} \pm \sim 0.30 \langle 110 \rangle_p^*$ as well as the $\mathbf{G} \pm \sim 0.30 \langle 110 \rangle_p^* + \frac{1}{2}\mathbf{c}_p^*$ positions of reciprocal space in the case of STS [5–8,11,20,22], it was considered important to first of all check whether or not the same incommensurate satellite reflections occur in the case of RVV. The absence of incommensurate satellite reflections at either of the $\mathbf{G} \pm \sim 0.30 \langle 110 \rangle_p^*$ or $\mathbf{G} \pm \sim 0.30 \langle 110 \rangle_p^* + \frac{1}{2}\mathbf{c}_p^*$ positions of reciprocal space is clear from the (a) $[001]_p$ and (b) $\langle 112 \rangle_p$ zone axis electron diffraction patterns (EDPs) shown in Fig. 3. In order to check whether or not they might condense out at a temperature below room temperature, equivalent low-temperature EDPs were also taken at liquid nitrogen temperature. Identical EDPs to those shown in Fig. 3, however, were again obtained, showing that RVV behaves quite differently from BTG, BTS, STS and BVS.

What was different about RVV at low temperature, however, was the presence of weak additional incommensurate satellite reflections, but this time running along the $\mathbf{c}^*$-direction of reciprocal space (see Fig. 4). That RVV is a $(3+1)$-$d$ incommensurately modulated structure at low temperature is apparent from the $\langle 110 \rangle_p$ and $\langle 010 \rangle_p$ zone axis EDPs shown in Fig. 4. (Note that the platey nature of the as-grown RVV
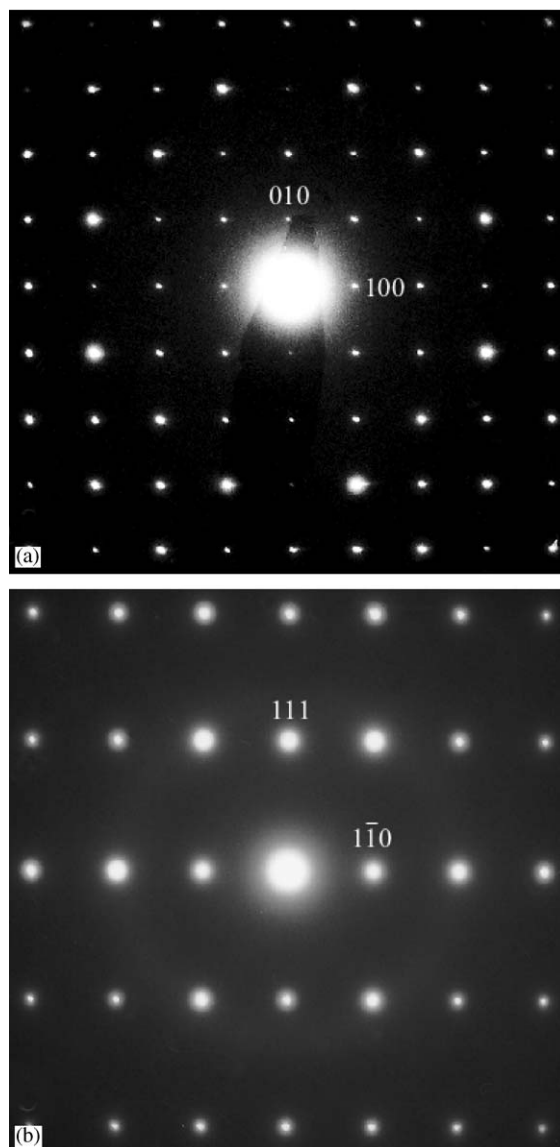


Fig. 3. (a) $[001]_p$ and (b) $\langle 112 \rangle_p$ (subscript p for parent) zone axis EDPs of $Rb_2V_3O_8$. Note the absence of either $\mathbf{G} \pm \sim 0.30 \langle 110 \rangle_p^*$ or $\mathbf{G} \pm \sim 0.30 \langle 110 \rangle_p^* + \frac{1}{2}\mathbf{c}_p^*$ satellite reflections.

crystals (see Fig. 2) in conjunction with the layered nature of the fresnoite structure meant that thin crushed grains were almost invariably aligned with the normal to the plates running close to the c-direction. Obtaining good-quality EDPs with $\mathbf{c}^*$ excited was thus a distinctly non-trivial task, particularly given the limited tilt available.) Indexation in Fig. 4a and b is with respect to the four basis vectors $M^* = \{\mathbf{a}_p^*, \mathbf{b}_p^*, \mathbf{c}_p^*, \mathbf{q} \sim 0.16[001]_p^*\}$. Note that only first-order harmonic satellite reflections are ever observed and that they are the strongest running along the $\mathbf{c}^*$-direction (see Fig. 4b), requiring that the atomic displacements responsible are also largely along the c-direction.

The characteristic extinction condition $F(h0lm) = 0$, unless h is even, and the four-fold related $F(0klm) = 0$ (unless k is even) (see Fig. 4b) require the presence of
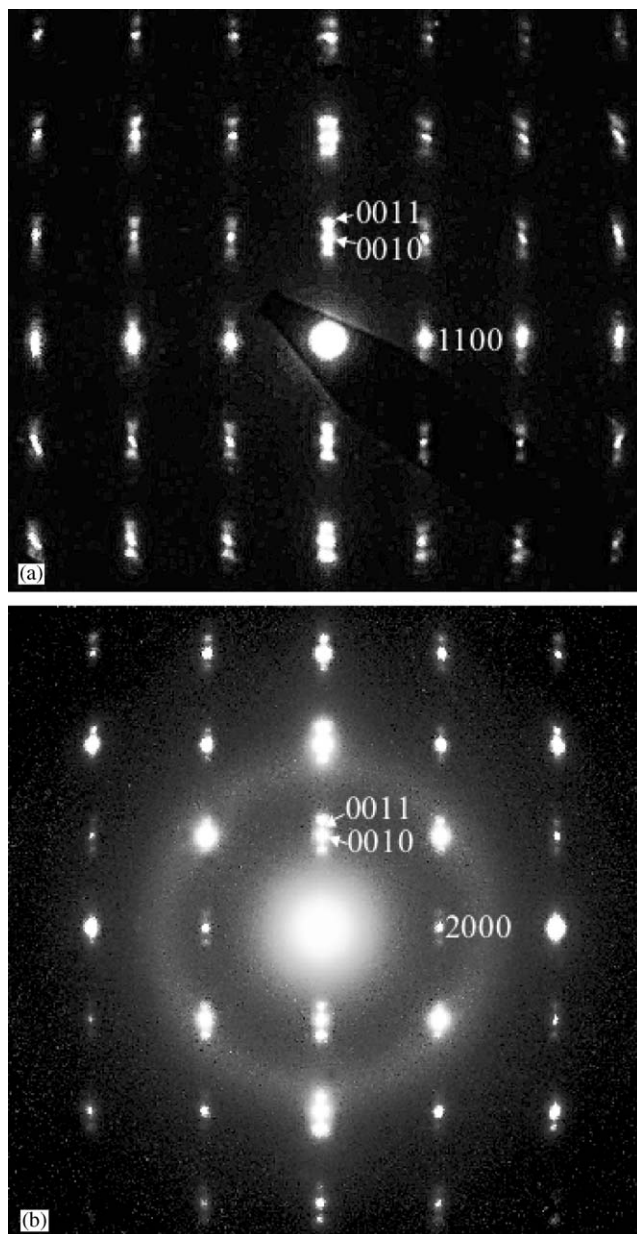
Fig. 4. Typical liquid nitrogen temperature (a) $\langle 110 \rangle$ and (b) $\langle 010 \rangle$ zone axis EDPs of the $(3+1)$-$d$ incommensurately modulated structure at low temperature. Indexation is with respect to the four basis vectors $M^* = \{\mathbf{a}_p^*, \mathbf{b}_p^*, \mathbf{c}_p^*, \mathbf{q} \sim 0.16[001]_p^*\}$.

the superspace symmetry operations $\{x_1 + \frac{1}{2}, -x_2 + \frac{1}{2}, x_3, x_4\}$ and $\{-x_1 + \frac{1}{2}, x_2 + \frac{1}{2}, x_3, x_4\}$, respectively. (The minimum possible superspace group symmetry is thus $Pba2(00\gamma)$-No. 32.1 in Table 9.8.3.5 of [25]). Assuming the additional presence of tertiary mirrors perpendicular to $\langle 110 \rangle_p$, the absence of any condition at these $\langle 110 \rangle_p$ axes (see Fig. 4a) implies the presence of the superspace symmetry operation $\{x_2 + \frac{1}{2}, x_1 + \frac{1}{2}, x_3, x_4\}$. Taken together, these experimental observations imply an overall $(3+1)$-$d$ superspace symmetry of $P4bm(00\gamma)$ (No. 100.1 in Table 9.8.3.5 of [25]).

Note that this $P4bm(00\gamma)$ superspace group symmetry severely constrains the form of the possible atomic shifts responsible. The $V^{4+}$ ions in the square pyramids, the oxygen ions capping these square pyramids as well as the oxygen ions bridging the $V_2O_7$ pyrovanadate group, for example, are each only allowed to shift along $\mathbf{c}$ (by a shift of the same amount within any one layer perpendicular to $\mathbf{c}$), while all the ions which fall on one or other tertiary mirror plane (Rb, the $V^{5+}$ ions in the tetrahedra and the oxygen ions capping these tetrahedra) are each forbidden shifts perpendicular to the local mirror plane they fall on (see Fig. 1).

## 3.2. DSC

Given that the incommensurate satellite reflections in Fig. 4 were not present at room temperature, DSC was performed in the range from liquid nitrogen temperature up to $+40^\circ$C with a rate of temperature change of $5^\circ$C per minute to see if a corresponding phase transition could be found. A well-defined phase transition was detected just below room temperature as shown in Fig. 5. This was the only phase transition detected over the whole temperature range. We therefore ascribe the phase transition to the condensation, or freezing out, of the incommensurate satellite reflections.

## 3.3. Lattice dynamical calculations and predicted RUM displacement eigenvector

Despite the fact that the particular 'soft' RUM mode [22,26,27] that condenses out in the cases of BTS, BTG, STS and BVS does not condense out in the case of RVV (see Fig. 3), it nonetheless should remain true that the energies associated with deformation of the constituent tetrahedral and square pyramidal polyhedral units in
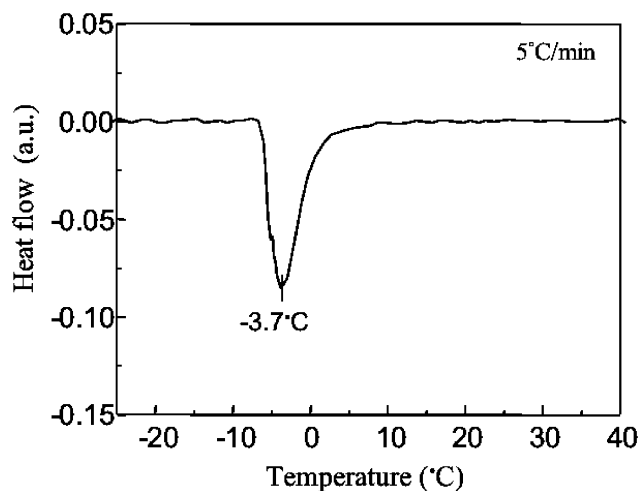


Fig. 5. DSC trace showing the existence of a well-defined phase transition just below room temperature.
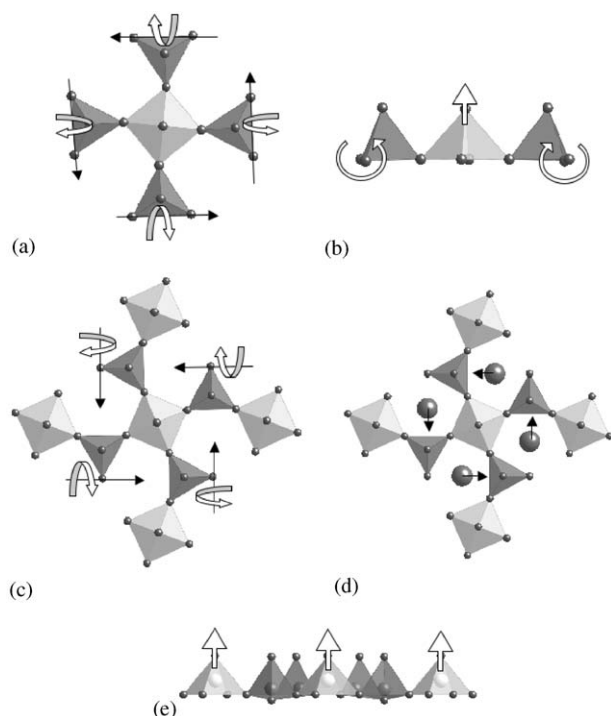
Fig. 6. (a, b) Schematic diagrams illustrating the two zero frequency RUM modes of distortion which can exist for any particular modulation wave vector of the ideal fresnoite framework structure. (a), (c) and (d) show projections along $\mathbf{c}_p$, while (b) and (e) show orthogonal projections. Only two of the four tetrahedra surrounding each TiO$_5$ square pyramid are shown in (b) for clarity reasons. (c) and (e) show orthogonal projections of the superspace symmetry allowed displacive shifts of the framework associated with the incommensurate modulation (the tetrahedral rotations are emphasized in (c) and the rigid body shifts of the square pyramids in (e)). The tetrahedra are understood to be rotating in a clock-wise sense about the basal plane rotation axes represented by the arrowed line in each case. The sense of polyhedral rotation is also indicated by the curved arrows. (d) shows the pattern of symmetry allowed, in-plane Rb ion shifts.

fresnoites should be rather larger than the energies associated with RUM-type rotation of these neighboring polyhedral units about a common vertex atom or the energies associated with the bonding interactions between the oxygens of the tetrahedra and the interstitial Rb ions. Consequently, the mode that has frozen out in the case of RVV should still be a RUM mode of the ideal fresnoite framework structure.

In the recent lattice dynamical investigation of the ideal fresnoite framework structure, it was shown that there exist six zero frequency RUM modes and two close to zero frequency quasi-RUM (q-RUM) modes for any modulation wave vector in addition to the specific RUM mode that condenses out in the cases of BTS, BTG, STS and BVS (see Fig. 5 of [22]). By contrast with this latter RUM mode, the former RUM modes are all associated with rotations of the constituent tetrahedra and square pyramids around in-plane (i.e. perpendicular to $c$) rotation axes (see Fig. 5 of [22]).

The above-proposed $P4bm(00\gamma)$ superspace group symmetry for RVV is only compatible with the first two of these six RUM modes (the first of these doubly degenerate RUM modes is shown in Fig. 6a and b). These two particular doubly degenerate RUM modes each involve tetrahedral rotation around specific (but different) O–O edges (one of these is shown in Fig. 6a), combined with rigid body translation of the enclosed VO$_5$ square pyramid along $\mathbf{c}$ (see Fig. 6b). From the RUM point of view, there exist two such modes for each wave vector because there exist two polyhedral groupings of the type shown in Fig. 6a per parent unit cell (cf. with Fig. 1). The superspace symmetry operations $\{x_1 + \frac{1}{2}, -x_2 + \frac{1}{2}, x_3, x_4\}$ and $\{-x_1 + \frac{1}{2}, x_2 + \frac{1}{2}, x_3, x_4\}$ constrain these two polyhedral groupings per parent unit cell to rotate and translate in phase as shown in Fig. 6c and e. The resultant tetrahedral rotation axes are thereby constrained to run through the O1 ions bridging the pyrovanadate group along the directions shown in Fig. 6c. Rotations (of the same magnitude) of the VO$_4$ tetrahedra about these rotation axes lead to rigid body translation of the attached VO$_5$ square pyramids along the $\mathbf{c}$-direction and buckling of the originally flat oxygen layers perpendicular to $\mathbf{c}$ (cf. Fig. 6e with Fig. 1b). Note that almost all the atoms of the framework thereby move predominantly along the $\mathbf{c}$-direction. (This is consistent with the refined 173 K anisotropic displacement parameters for RVV reported below, where $U_{33}$ for most framework ions is significantly larger than $U_{11}$ or $U_{22}$—see Table 1.)

Note that the the $P4bm(00\gamma)$ superspace group symmetry also allows the Rb ions within any one (001) layer to move in phase along the $\mathbf{c}$-axis direction as well as to have an in-plane displacive component (but only along the directions shown in Fig. 6d). (The RUM model gives no idea as to the magnitude of these shifts of the interstitial Rb ions as it focuses solely on the corner-connected tetrahedral and square pyramidal 2-$d$ polyhedral sheets. The fact that the refined Rb anisotropic displacement ellipsoid (see Table 1 and Fig. 7a) is relatively strongly peaked orthogonal to the shifts shown in Fig. 6d suggests that it cannot be responsible for the observed incommensurate modulation.)

Within any one layer perpendicular to $\mathbf{c}$, the atomic displacements associated with the proposed condensed RUM mode are then determined by only one parameter, the amplitude of the in-plane tetrahedral rotations about the axes shown in Fig. 6c. The amplitude of this rotation, $R$, for any one particular (001) layer can then formally be written in the form $R(l\mathbf{c}) = R\cos(2\pi\mathbf{q} \cdot l\mathbf{c})$ where $\mathbf{q} \sim 0.16\,\mathbf{c}^*$ and $l\mathbf{c}$, $l$ an integer, simply labels the various layers perpendicular to $\mathbf{c}$ (see Fig. 1) (Fig. 6e corresponds to a rotation amplitude $R$ of 7°). The phase shift of the overall atomic displacement pattern (shown in Fig. 6c and e) from one (001) layer to the next is then given by $2\pi\mathbf{q}.\mathbf{c}$, which for $\mathbf{q} \sim 0.16\mathbf{c}^*$ gives $\sim 60°$, i.e.

Table 1
Anisotropic displacement parameters ($\text{Å}^2$) obtained from the 173 K refinement of X-ray single-crystal diffraction data of $Rb_2V_3O_8$

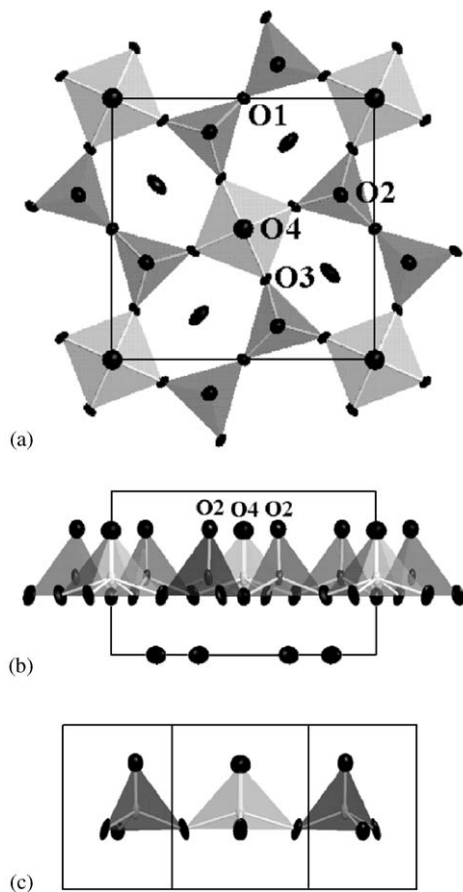| Atom | $U_{11}$ | $U_{22}$ | $U_{33}$ | $U_{12}$ | $U_{13}$ | $U_{23}$ |
|---|---|---|---|---|---|---|
| Rb | 0.0140(2) | 0.0140(2) | 0.0112(3) | −0.0080(2) | −0.0005(3) | −0.0005(3) |
| V1 | 0.0027(4) | 0.0027(4) | 0.0081(8) | 0.00000 | 0.00000 | 0.00000 |
| V2 | 0.0022(3) | 0.0022(3) | 0.0094(6) | 0.0000(4) | −0.0007(4) | −0.0007(4) |
| O1 | 0.006(2) | 0.006(2) | 0.012(3) | −0.001(3) | 0.00000 | 0.00000 |
| O2 | 0.0088(16) | 0.0088(16) | 0.012(2) | 0.001(2) | 0.0002(14) | 0.0002(14) |
| O3 | 0.0059(16) | 0.0048(16) | 0.0155(18) | 0.0023(14) | 0.0026(15) | −0.0031(14) |
| O4 | 0.014(2) | 0.014(2) | 0.012(3) | 0.00000 | 0.00000 | 0.00000 |



Fig. 7. Unit cell of RVV at 173°K in projection along (a) the $c$-axis, (b) the $b$-axis, and (c) along $\sim$[410] with displacement ellipsoids on the 95% probability level and coordination polyhedra superimposed.

$\sim$ every three layers or so, the sense of rotation of the tetrahedral and the shift direction of the $VO_s$ square pyramids reverse sign. Such a RUM displacement eigenvector is quite compatible with the observed superspace group symmetry, as well as with the fact that the incommensurate satellite reflections are strongest along the **c**-direction (provided the magnitude of the symmetry allowed in-plane Rb ion displacements shown in Fig. 6d is small). The magnitude of the rotations and shifts involved, however, can only be determined via a full $(3+1)$-$d$ incommensurate structure refinement (see, e.g. [6]), although the weakness of the

observed satellite reflections in Fig. 4 suggests that the overall amplitude must be quite small.

### 3.4. Single-crystal average structure X-ray refinement

Just such a $(3+1)$-$d$ incommensurate structure refinement was attempted with a data set acquired at 173 K. Unfortunately, the weak incommensurate satellite reflections were not detected. Hence, the data were refined in 3D focusing on the refined anisotropic displacement ellipsoids to gain additional insight as to the atomic displacements responsible for the observed modulation. These refined anisotropic displacement factors are given in Table 1, while the refined average structure fractional co-ordinates are given in Table 2 and the crystal data collection details in Table 3. (Note that the fractional co-ordinates given in Table 2 can be transformed into the setting used in Refs. [10] and [23] via the transformation $-x$, $-y$, $0.65-z$).

Inspection of the refined anisotropic displacement ellipsoids (see Fig. 7) reveals several important details when considering that these parameters are just another (less correct, but in the present case the only feasible) way to assess the atomic displacements associated with the formation of the modulated structure. From the condensed RUM model of Fig. 6, one would expect the anisotropic displacement ellipsoids of the V1, V2, O3 and O4 ions to be strongly peaked along the $c$-direction, with that of the O2 ion being rather more isotropic (see Fig. 7). Experimentally, this is essentially true for the V1, V2, O2 and O3 ions with the refined displacement ellipsoids, suggesting that the amplitude of the presumed rigid body shift of the $V_1O_5$ square pyramids along $c$ is associated with the condensed mode being $\sim 0.1\,\text{Å}$. The displacement ellipsoid for the O4 ion is rather more isotropic (see Fig. 7b), suggesting the need for additional thermally excited RUM modes (such as those shown in Fig. 5c and d of [22]) allowing basal plane motion of the O4 ion. This would also provide a potential explanation for the larger refined magnitude of $U_{33}$ for O3 relative to that for V1. (It should be borne in mind that a condensed RUM mode of the type shown in Fig. 6 does not preclude the simultaneous thermal excitation of the other zero frequency RUM modes shown in Fig. 5 of

[22]; indeed the refined anisotropic displacement ellipsoids provide indirect evidence for their thermal excitation). Likewise, peaked along the *c* ellipsoid of the O1

Table 2
Refined fractional co-ordinates of $Rb_2V_3O_8$ at 173 K

| Atom | Wyck. | $x$ | $y$ | $z$ |
|---|---|---|---|---|
| Rb | 4*c* | 0.33050(5) | 0.83050(5) | 0 |
| V1 | 2*a* | 0 | 0 | 0.5322(4) |
| V2 | 4*c* | 0.13351(8) | 0.63351(8) | 0.5271(3) |
| O1 | 2*b* | 0 | 1/2 | 0.6450(12) |
| O2 | 4*c* | 0.1294(4) | 0.6294(4) | 0.2323(11) |
| O3 | 8*d* | 0.3078(4) | 0.5852(4) | 0.6360(7) |
| O4 | 2*a* | 0 | 0 | 0.2423(14) |

Table 3
Crystal data and data collection parameters for $Rb_2V_3O_8$

| *Crystal data* | |
|---|---|
| Chemical formula | $Rb_2V_3O_8$ |
| Formula weight (g/mol) | 451.8 |
| Cell setting | Tetragonal |
| Space group | *P4bm* |
| $a$ (Å) | 8.9229(18) |
| $c$ (Å) | 5.5014(11) |
| $V$ (Å³) | 438.01(15) |
| Formula units | 2 |
| Density (g/cm³) | 4.6869 |
| Crystal size | $0.1 \times 0.1 \times 0.05 \, mm^3$ |
| Crystal colour | Black |
| | |
| *Data collection* | |
| Diffractometer | STOE IPDS |
| Data-acquisition temperature (K) | 173 |
| Radiation type | Mo$K\alpha$ |
| Wavelength (Å) | 0.71073 |
| No. of images | 200 |
| $\varphi$ range | 0–200° |
| $2\theta$ range | 3.2–24.1° |
| $\mu$ (mm⁻¹) | 19.4 |
| Data-collection method | Phi rotation scans |
| Absorption correction | Numerical from crystal shape |
| $T_{min}$, $T_{max}$ | 0.098, 0.194 |
| No. of measured reflections | 2364 |
| No. of observed reflections | 2005 |
| No. of independent reflections | 386 |
| Criterion for observed reflections | $I \geqslant 3\sigma(I)$ |
| $R_{int}$ | 0.057 |
| *h, k, l, m, n* range | $-10 \leqslant h \leqslant 10$ |
| | $-10 \leqslant k \leqslant 9$ |
| | $-6 \leqslant l \leqslant 6$ |
| | |
| *Refinement* | |
| Refinement on | $F$ |
| $R$-factors of all observed reflections $R$, w$R$ | 0.019, 0.049 |
| Goodness of fit | 1.01 |
| No. of reflections used in refinement | 386 |
| No. of parameters used in refinement | 37 |
| Weighting scheme | $1/(\sigma^2(F) + 0.0016F^2)$ |
| Residual electron density: max., min. (e/Å³) | 0.61, −0.55 |

ion suggests thermally excited RUM modes (such as those shown in Fig. 5e and f of [22]).

Summarizing then, the shape of the refined displacement ellipsoids is, we believe, compatible with the RUM picture developed above, since rigid-body movements of the polyhedra are possible within the limits of the ellipsoids and also the toggling of polyhedra necessary for the rigid movement along *c* (cf. Fig. 7b) is indicated (Fig. 7c). The $\sim \pm 0.15$ Å shifts of the Rb ions (perpendicular to the local tertiary mirror plane on which they lie) implied by the refined Rb displacement ellipsoid (see Fig. 7a) are clearly significant, but cannot be associated with the condensed incommensurate modulation (as a result of the observed superspace group symmetry) and hence must be thermally excited. It is possible that these Rb shifts might themselves condense out upon further cooling below liquid nitrogen temperature.

### 3.5. Bond valence sum considerations

In earlier papers [6,8,11], the cause and even extent of the observed modulation amplitude in BTG, BTS, STS and BVS has been attributed to the extent of "under-bonding" of the interstitial cations in the parent *P4bm* fresnoite structure. In large amplitude modulated BTG, for example, the two interstitial Ba ions in the *Cmm*2 average structure give bond valence sums of 1.700 and 1.816, i.e. they are under-bonded by 15% and 9.2%, respectively. Similarly, the interstitial Sr ion in the parent structure of STS, another large amplitude modulated fresnoite, is under-bonded by 18.9%. By contrast, the interstitial Ba ion in the fresnoite "parent" structure of BTS is only under-bonded by $\sim 1.6$% and has a much smaller modulation amplitude.

In the current case of $Rb_2V_3O_8$ (see Table 4), the interstitial Rb ion is, by contrast, over-bonded (by $\sim 9.4$%). This provides a clear crystal chemical distinction between vanadate fresnoites and BTG, STS, BTS and BVS. Presumably, the initial over-bonding of the interstitial ions in the case of the vanadate fresnoites is responsible for suppressing the particular condensed

Table 4
Bond valence sums (or apparent valences, AVs [28]) for the constituent ions of the refined 173 K average structure of $Rb_2V_3O_8$ (co-ordinates from Table 2)

| Atom label | AV |
|---|---|
| Rb | 1.094 |
| V1 | 4.147 |
| V2 | 5.115 |
| O1 | 2.345 |
| O2 | 2.123 |
| O3 | 2.077 |
| O4 | 1.667 |

RUM mode observed in the cases of BTG, STS, BTS and BVS. It does not, however, appear to be primarily responsible for driving the condensation of the observed incommensurate modulation.

## 4. Conclusion

Electron diffraction has shown that the low-temperature structure of $Rb_2V_3O_8$ is $(3 + 1)$-$d$ incommensurately modulated with a primary modulation wave vector given by $\mathbf{q} \sim 0.16\mathbf{c}^*$. The observed characteristic extinction conditions imply a $P4bm(00\gamma)$ superspace group symmetry. A condensed RUM mode involving $VO_4$ tetrahedral rotation around in-plane rotation axes combined with rigid body $\mathbf{c}$-axis shifts of $VO_5$ square pyramids is suggested to be responsible. This condensed RUM mode is quite distinct from the condensed RUM mode involving polyhedral rotation around $\mathbf{c}$, which occurs in the cases of BTS, BTG, STS and BVS.

## Acknowledgments

## References

[1] J.T. Alfors, M.C. Stinton, R.A. Matthews, A. Pabst, Amer. Mineralogist 50 (1965) 314–340.

[2] R. Masse, J.-C. Grenier, A. Durif, Bull. Soc. Franc. Mineral. Crystallogr. 90 (1967) 20–23.

[3] P.B. Moore, S.J. Louisnathan, Z. Kristallogr. 130 (1969) 438–448.

[4] M. Kimura, K. Doi, S. Nanamatsu, T. Kawamura, Appl. Phys. Lett. 23 (1973) 531–532.

[5] K. Iijima, F. Marumo, M. Kimura, T. Kawamura, J. Chem. Soc. Japan 10 (1981) 1557–1563.

[6] T. Höche, S. Esmaeilzadeh, R. Uecker, S. Lidin, W. Neumann, Acta Crystallogr. B 59 (2003) 209–216.

[7] T. Höche, C. Rüssel, W. Neumann, Solid State Commun. 110 (1999) 651–656.

[8] T. Höche, W. Neumann, S. Esmaeilzadeh, R. Uecker, M. Lentzen, C. Rüssel, J. Solid State Chem. 166 (2002) 15–23.

[9] A. Feltz, S. Schmalfuss, H. Langbein, M. Tietz, Z. Anorg. Allg. Chem. 417 (1975) 125–129.

[10] G. Liu, J.E. Greedan, J. Solid State Chem. 108 (1994) 267–274.

[11] T. Höche, S. Esmaeilzadeh, R.L. Withers, H. Schirmer, Z. Krist. 218 (2003) 788–794.

[12] J. Galy, A. Carpy, Acta Crystallogr. B 31 (1975) 1794–1795.

[13] G. Liu, J.E. Greedan, J. Solid State Chem. 114 (1995) 499–505.

[14] E. Andrukaitis, P.W.M. Jacobs, J.W. Lorimer, Can. J. Chem. 68 (1990) 1283–1292.

[15] H. Schmid, P. Genequand, H. Tippmann, G. Pouilly, H. Guedu, J. Mater. Sci. 13 (1978) 2257–2265.

[16] A. Halliyal, A.S. Bhalla, S.A. Markgraf, L.E. Cross, R.E. Newnham, Ferroelectrics 62 (1985) 27–38.

[17] S.A. Markgraf, A. Halliyal, A.S. Bhalla, R.E. Newnham, Ferroelectrics 62 (1985) 17–26.

[18] J. Choi, Z.T. Zhu, J.L. Musfeldt, G. Ragghianti, D. Mandrus, B.C. Sales, J.R. Thompson, Phys. Rev. B 65 (2001) 054101: 1–054101:6.

[19] N. Ye, Q. Chen, B. Wu, C. Chen, J. Appl. Phys. 84 (1998) 555–558.

[20] S.A. Markgraf, A. Bhalla, Phase Transit. 18 (1989) 55–76.

[21] S.A. Markgraf, C.A. Randall, A. Bhalla, R.J. Reeder, Solid State Commun. 75 (1990) 821–824.

[22] R.L. Withers, Y. Tabira, Y. Liu, T. Höche, Phys. Chem. Miner. 29 (2002) 624–632..

[23] M.L. Ha-Eierdanz, U. Müller, Z. Anorg. Allg. Chem. 613 (1992) 63–66.

[24] B.C. Sales, M.D. Lumsden, S.E. Nagler, D. Mandrus, R. Jin, Phys. Rev. Lett. 88 (2002) 095901:1–095901:4.

[25] T. Janssen, A. Janner, A. Looijenga-Vos, P.M. de Wolff, Incommensurate and commensurate modulated structures, in: A.J.C. Wilson (Ed.), International Tables for Crystallography, Vol. C, Kluwer Academic Publishers, Dordrecht, 1995, pp. 797–835.

[26] K.D. Hammonds, M.T. Dove, A.P. Giddy, V. Heine, Am. Mineralogist 79 (1994) 1207–1209.

[27] K.D. Hammonds, M.T. Dove, A.P. Giddy, V. Heine, B. Winkler, Am. Mineralogist 81 (1996) 1057–1079.

[28] N.E. Brese, M. O'Keeffe, Acta Crystallogr. B 47 (1991) 192–197.